A slow slip event in the south central Alaska Subduction Zone and related seismicity anomaly

Meng Wei,[1] Jeffrey J. McGuire,[1] and Eliza Richardson[2]

Received 10 May 2012; revised 3 July 2012; accepted 5 July 2012; published 11 August 2012.

[1] We detected a slow slip event in the south central Alaska Subduction Zone by analyzing continuous GPS data from the Plate Boundary Observatory (PBO) network. The slow slip event started in early 2010 at a depth of 35 km beneath the Cook Inlet, near the down-dip end of the locked zone, and is ongoing as of November 2011 with an accumulated magnitude of M_w 6.9. Analysis of the earthquake catalog in the same area using the stochastic Epidemic Type Aftershock Sequence model (ETAS) shows a small but detectable seismicity increase during the slow slip event. We also find a change in seismicity rate around 1998, that may suggest an earlier slow slip event in the same region. Slow slip events in Alaska appear more widespread than previously thought but have remained undetected due to their long durations, the time intervals between them, and the limited time records from the continuous GPS. **Citation:** Wei, M., J. J. McGuire, and E. Richardson (2012), A slow slip event in the south central Alaska Subduction Zone and related seismicity anomaly, *Geophys. Res. Lett.*, *39*, L15309, doi:10.1029/2012GL052351.

1. Introduction

[2] With the advance of geodetic observation technology, especially the development of continuous GPS networks, slow slip events (SSEs) on faults have been observed in many places [*Schwartz and Rokosky*, 2007]. SSEs – also termed "slow earthquakes," "silent earthquakes," "creep events," "aseismic strain transients," or "slip transients" – refer to slow fault motion that does not radiate significant energy as seismic waves. In contrast to continuous creep below the seismogenic zone, these events have a finite duration, usually ranging from a few days to years and typically involve fault-slip at rates well above the long-term (geologic) slip-rate of the fault. Slow slip events can trigger swarms of small to moderate earthquakes [*Ozawa et al.*, 2003] as well as non-volcanic tremor [e.g., *Beroza and Ide*, 2011, and references therein]. They themselves can be triggered by the passage of surface waves [*Itaba and Ando*, 2011] or the static stress change caused by ordinary fast-rupturing earthquakes [*Du et al.*, 2003]. Although SSEs have been observed in many places including Cascadia, Southeast Japan, New Zealand, and Salton Trough, California, our knowledge of the mechanism of SSEs and the interaction between SSEs, tremor and earthquakes is still limited by the number of observed cases. Quantifying the variability in the duration and mechanical properties of slow slip events among different subduction zones will help constrain the physical conditions on the thrust interface that promote the occurrence of SSEs.

[3] Recently, a new algorithm termed the Network Strain Filter (NSF), has been developed to detect strain transients in large GPS networks [*Ohtani et al.*, 2010]. The Network Strain Filter is built on the Network Inversion Filter (NIF) [*Segall and Matthews*, 1997; *McGuire and Segall*, 2003; *Fukuda et al.*, 2004, 2008]. The NIF is designed to study established deformation sources, such as individual faults with known geometry or previously identified magma chambers, and it uses information (Green's functions) about the signals expected from those identified sources to search for transients. In contrast, the NSF is designed to search over large areas with multiple and/or unknown sources of transient deformation. To achieve this flexibility it employs spatial wavelets rather than Green's functions to represent the strain transients.

[4] In this paper, we report the detection of a slow slip event in the South Central Alaska Subduction Zone by applying the NSF to the PBO GPS data in this region (Figure 1). The slip transient started in early 2010 and has not ceased as of November 2011; its accumulated magnitude is about M_w 6.9. We also observe a small seismicity increase that coincides in time and space with the detected SSE. This SSE occurs in the same depth range as an earlier slow slip event during 1998–2001, located 300 km to the northeast [*Ohta et al.*, 2006].

2. GPS Data

[5] We used PBO level 2 GPS products for our analysis [*Anderson*, 2004]. These provide daily position estimates and covariance for the entire PBO network in the Stable North America Reference Frame (http://unavco.org/community_science/workinggroups_projects/snarf/snarf.html). We focused on south central Alaska near Kodiak Island and the Kenai Peninsula, adjacent to the 1964 M_w 9.2 earthquake rupture area [*Kanamori*, 1977; *Christensen and Beck*, 1994; *Johnson et al.*, 1996] and near the 1998–2001 SSE, the only known SSE in Alaska previous to this study [*Ohta et al.*, 2006]. In our study region (latitude 54° to 65°, longitude −160° to −140°), more than 54 continuous stations have more than 4 years of data, primarily beginning in late 2006. To ensure relatively uniform station coverage over time, we used data from Jan. 1, 2007 to November 30, 2011, such that the number of observed daily epochs at individual stations ranges from 902 to 1760 with a mean of 1498. Because we focused on large-scale tectonic deformation, we only used

[1]Woods Hole Oceanographic Institution, Woods Hole, Massachusetts, USA.
[2]Department of Geosciences, Pennsylvania State University, University Park, Pennsylvania, USA.

Corresponding author: M. Wei, Woods Hole Oceanographic Institution, 266 Woods Hole Rd., MS 24, Woods Hole, MA 02543, USA. (mwei@whoi.edu)

0094-8276/12/2012GL052351

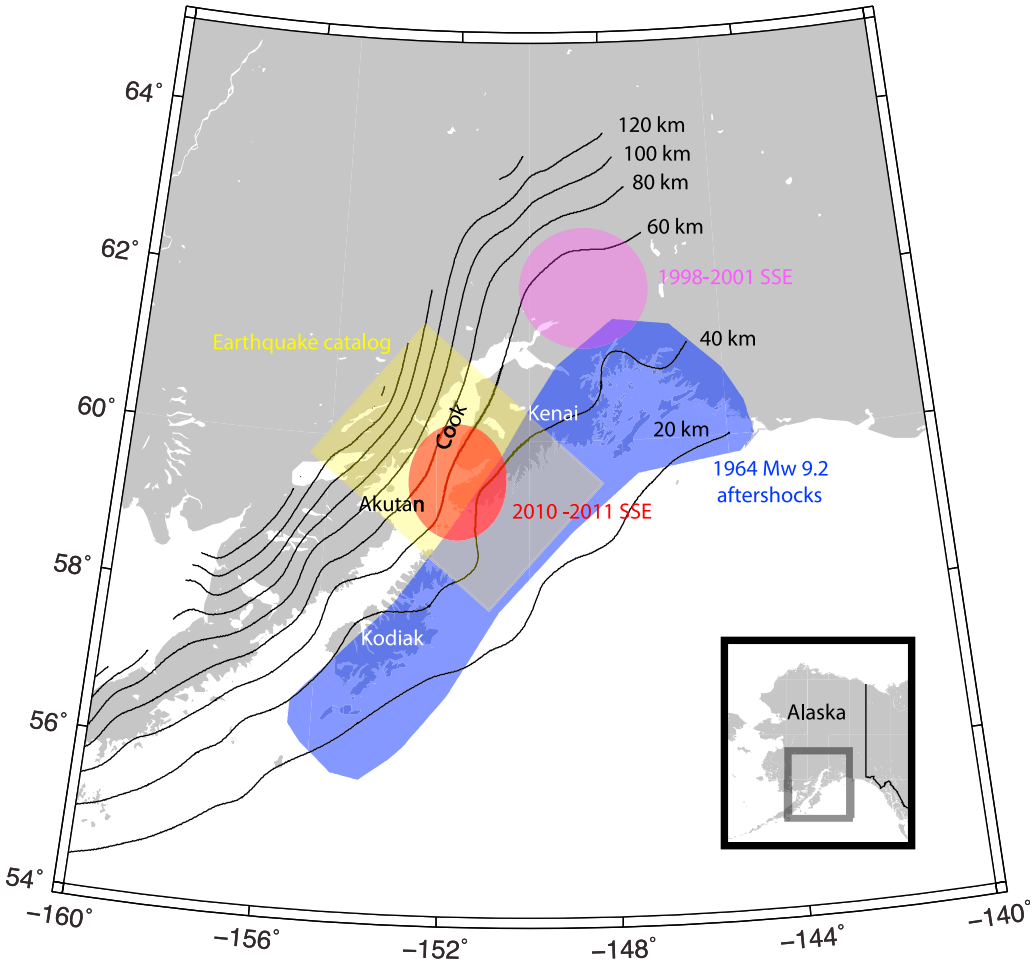

Figure 1. Map of south central Alaska. Dark purple shows the aftershock area of the 1964 earthquake by *Furumoto* [1965]. Light purple area is the region of the slow slip event between 1998 and 2001 reported by *Ohta et al.* [2006]. Red region shows the slow slip event in this study. Yellow box covers the area used in the seismicity anomaly analysis. Black solid lines are interface depths from Slab 1.0 [*Hayes et al.*, 2012].

one of the available stations on the Akutan Island Volcano (Figure 1).

3. Detection of Transients With the Network Strain Filter

[6] Here we introduce the NSF method used to analyze the GPS data. For a detailed description of the method, see *Ohtani et al.* [2010]. The NSF assumes that GPS time series are the summation of several tectonic and non-tectonic processes:

$$x(t) - x(t_0) = v \cdot (t - t_0) + u(x,t) + L(x, t - t_0) + A \cdot \sin\left(\frac{2\pi t}{T}\right) + B \cdot \cos\left(\frac{2\pi t}{T}\right) + Ff(t) + \varepsilon$$

$$\varepsilon \sim N(0, \sigma^2)$$

where ν is the secular velocity, u is the transient field, L is site-specific noise from local benchmark instability, which is modeled as a Brownian random walk with scale parameter (unit length time$^{-1/2}$) [*Wyatt*, 1989]. The sine and cosine represents the seasonal variations. We only analyzed the horizontal components of the GPS data because they have smaller seasonal terms and white noise, and hence a much better signal to noise ratio. $Ff(t)$ is the reference frame error, where F is a Helmert transformation and $f(t)$ is a vector of rigid body translations, rotations, and a scale factor [*Miyazaki et al.*, 2003]. Reference frame errors are sometimes called common mode motion because they appear in all the stations. ε is the observation error, which is assumed to be normally distributed with zero mean and covariance σ^2. We use constant covariance of observation error for all GPS stations.

[7] Many GPS time series record seasonal signals, which are believed to result from a combination of soil moisture, hydrologic and atmospheric loading, and antenna mismodeling. Following *Murray and Segall* [2005], we modeled the seasonal term as a sum of sine and cosine terms with time-varying amplitudes.

[8] The transient tectonic displacement fields $u_i(x, t)$ are expanded in spatial basis functions $B_{im}(x)$ with time-varying coefficients $c_m(t)$

$$u_i(x,t) = \sum_m^M B_{im}(x) c_m(t)$$

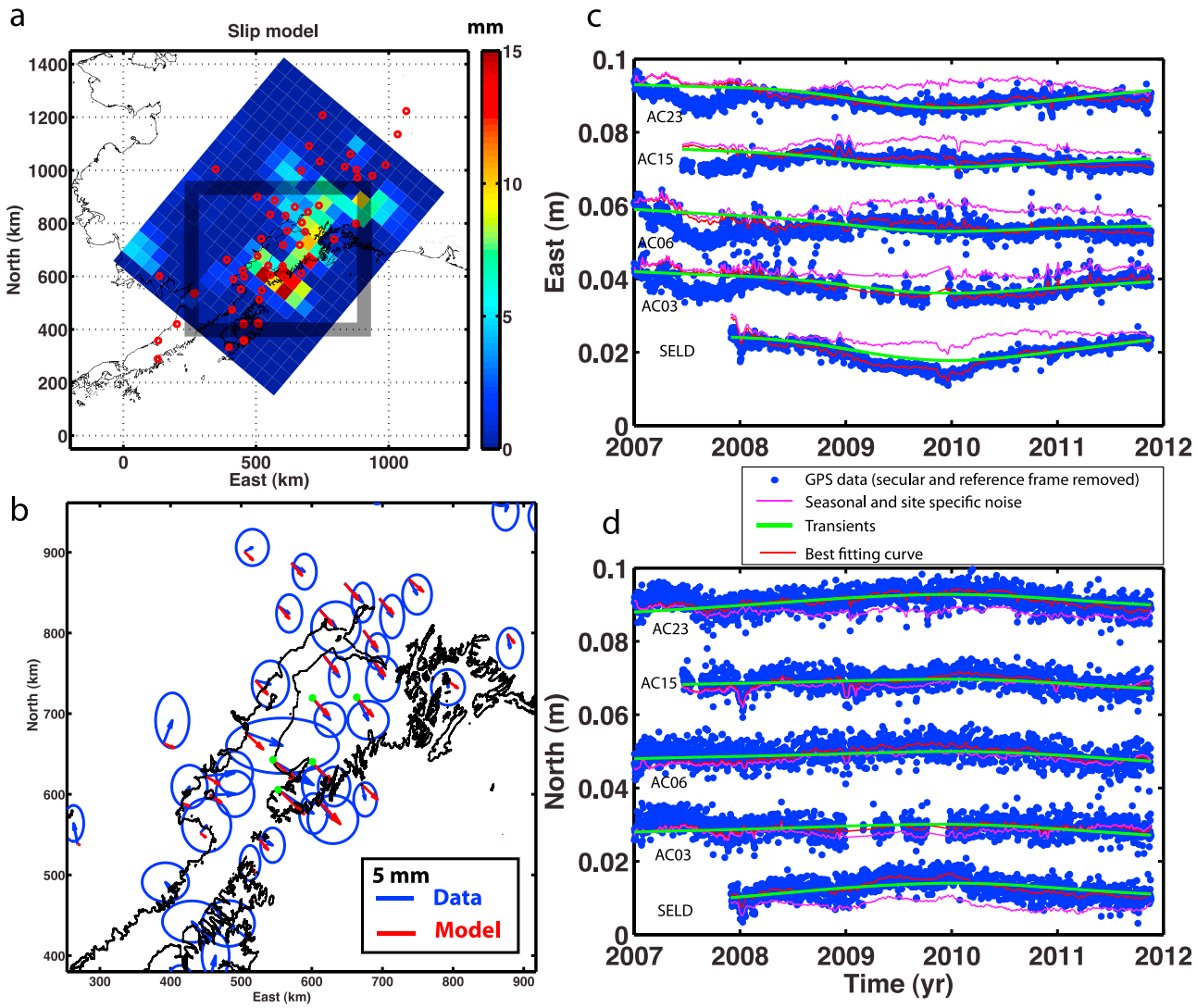

Figure 2. (a) Slip model of the 2010 slow slip event. Red circles are GPS stations. Gray box is the area of Figure 2b. (b) GPS data and best fitting model in the horizontal components for time period 1 Jan. 2010–30 Nov. 2011. Green dots are the five stations shown in c and d. Ellipses are the 1σ error. (c, d) GPS time series of five stations with slip transient near the Kenai Peninsula.

where i is the displacement component index and M is the number of basis functions. The time-varying coefficients $c_m(t)$ are modeled as stochastic processes. To better represent localized deformation, we use wavelets as the basis function. The minimum and maximum wavelet scales are determined as follows. The maximum scale is set by the geographic size of the geodetic array. The choice of minimum scale wavelet is determined by the station spacing. Choosing a minimum scale that is too small results in mapping local noise processes into deformation, leading to spurious estimates of transient deformation. We only keep wavelets that cover at least 4 stations in the expansion (Figure S1 in the auxiliary material).[1]

[9] The NSF uses an extended Kalman filter to estimate all the time-varying unknowns, including the coefficients of transient fields, secular motion, benchmark motion, seasonal variations, reference frame error, and a temporal smoothing parameter. A prior state vector (initial values and covariance matrix) corresponding to zero transient slip-rate is specified to initialize the filter. The extended Kalman filter updates the state vector and its covariance matrix after each epoch. Additionally, when appropriate we modify the process noise covariance matrix at pre-determined epochs to incorporate offsets due to either co-seismic deformation or the reinstallation of antennae at particular sites. After reaching the final epoch, a back-smoothing filter, with effectively fixed values for the secular motion and temporal smoothing parameter, is applied to determine the final optimal estimates of the state vector given the entire data time series.

4. Results

[10] While the vast majority of the GPS time series in the region can be explained by the secular motion, reference frame, and seasonal components of the model, the NSF

[1]Auxiliary materials are available in the HTML. doi:10.1029/2012GL052351.

identified a period of transient deformation that was localized near Kodiak Island and the Kenai Peninsula (Figure 2b). Results from five stations near the maximum surface displacements show that the signal is spatially and temporally coherent (Figures 2c and 2d). A velocity change occurs in both the east and north components of these sites at the beginning of 2010 with displacements ranging from 2 to 5 mm over 23 months. The maximum displacement (5 mm in 23 months) was recorded at station SELD (Figure S2) on the southern end of the Kenai Peninsula. Due to the limited length of data records (~5 years), there is an ambiguity as to which time period is 'the anomaly' and which corresponds to the predominately long-term interseismic behavior. The long-term trenchward motion observed by earlier geodetic surveys has been interpreted as postseismic creep on the down-dip portion of the plate interface after the 1964 megathrust earthquake [*Zweck et al.*, 2002]. In 2010, it is clear that the deformation rate recorded by these five stations increased. For example, at station SELD, starting in 2010 the deformation rate increased by 0.3 cm/yr in the southeast direction (Figure S2). Thus, the increased deformation rate we observe may indicate a transient increase in slip-rate on the plate interface and/or an expansion of the creeping area near the down-dip section of the thrust interface.

[11] Horizontal seasonal variations in most stations are small (<1 mm peak to trough), including at the stations that show slow slip event signals. Stations AB41, AC08, AC38 (Figure S3), however, show very strong seasonal variations with >15 mm peak to trough. Stations AC27 and AC76 show moderate (~10 mm) seasonal variations, but these five stations are distant (>100 km) from the 2010 SSE (compare Figures 1 and S3). Hence we do not expect the seasonal variations at these sites to significantly influence our results.

5. Dislocation Modeling

[12] After the deformation transient was identified in the GPS data, we verified that the signal could result from a change in slip-rate along the subducting plate interface. The transient displacement field of the 23 months following 2010.0, as estimated by the NSF, was modeled by slip on a planar fault in an elastic homogeneous half space [*Okada*, 1985] that dips 12° from the trench [*Hayes et al.*, 2012]. Even though complex fault plane geometries have been proposed for this region [*Zweck et al.*, 2002], the spatial sampling of PBO stations in Alaska is too sparse for this study to distinguish between a planar fault model and a more complicated one.

[13] Slip inversions using surface deformation data are well-established techniques [*Murray et al.*, 2001; *Fialko et al.*, 2005]. A homogeneous elastic half-space model is used to estimate the dip-slip components at depth using least squares fitting of the surface deformation data (Figures 2a and 2b). Since the problem is inherently non-unique, additional constraints are added to regularize the inversion. We prohibited dip slip away from trench by using a Coleman algorithm, which is the default in MATLAB function "lsqlin" [*Coleman and Li*, 1996]. We assume the slip distribution is to some degree smooth and use a Laplacian smoothness constraint that was controlled through a weighting parameter. The root mean square misfit of the model is inversely related to the smoothness weighting parameter, which is a classic trade-off [*Fialko et al.*, 2005]. We use cross validation to choose the optimal value for the smoothness parameter [*Murray et al.*, 2001] (Figure S4).

[14] The inversion results demonstrate that the transient deformation field can be explained by the slip-distribution shown in Figure 2a, which has a maximum slip of 17 mm beneath the Cook Inlet. Although the displacement is relatively small, it covers a large region, so the accumulated magnitude reaches *Mw* 6.9 in 23 months. Most GPS data are well fit by the model except for stations on Kodiak Island (AC02, AC34, AC38 and AC67) and 5 stations in the most western part of the region.

6. ETAS Modeling of Seismicity

[15] Slow slip events have been demonstrated to trigger small and moderate earthquakes in various tectonic environments including subduction zones [*Ozawa et al.*, 2003; *Llenos et al.*, 2009]. We searched for any variation of seismicity related to this SSE, using the stochastic Epidemic Type Aftershock Sequence model (ETAS) [*Ogata*, 1988; *Llenos et al.*, 2009]. Based on the ETAS model, the seismicity rate of a certain region at time t is

$$\lambda(t) = \mu + \sum_{t_i \le t} \frac{K e^{\alpha(M_i - M_c)}}{(t - t_i + c)^p}$$

where μ is the background seismicity rate, c and p are the Omori decay parameters, α is related to the efficiency of an earthquake of a given magnitude at generating aftershocks, K reflects the aftershock productivity of a mainshock, M_i is the magnitude of earthquakes in a catalog and M_c is the magnitude completeness of the catalog. These parameters are generally estimated for a region using maximum likelihood estimation from the observed earthquake times and magnitudes during a training time period. Then other time periods can be tested for deviations from the predicted rate of seismicity that indicate either quiescence or elevated earthquake rates.

[16] We used the Advanced National Seismic System (ANSS) earthquake catalog data to assess whether any anomalous seismic behavior occurred in concurrence with the detected SSE for the area is shown in Figure 1 (yellow box). We confined our analysis to slab seismicity and excluded shallower seismicity (<30 km depth), much of which reflects transient volcanic activity.

[17] We detected a small seismicity rate change in mid-2010, during the timeframe of the SSE (Figure 3b). However, analyzing data using the ETAS model is challenging in this region due to lack of large aftershock sequences in the depth range of the slab (30–70 km), and because the catalog is not complete in the time period around the M_w 7.9 Denali earthquake of 3 November, 2002. In order to circumvent the Denali problem, we used 1990–1995.5 as the training period for calculating ETAS parameters. Given the lack of large aftershock sequences, there is a significant trade-off between the different parameters that results in a relatively flat likelihood space where parameter combinations that correspond to low overall aftershock productivity are favored. To reduce the trade-offs, we fixed p = 1.0 and optimized the other parameters, which had optimal values of α = 4.9, μ = 0.89/day, K = .21, c = .018. The unrealistically high value of α is just one solution that results in relatively low overall aftershock productivity. However, these values provide a good fit

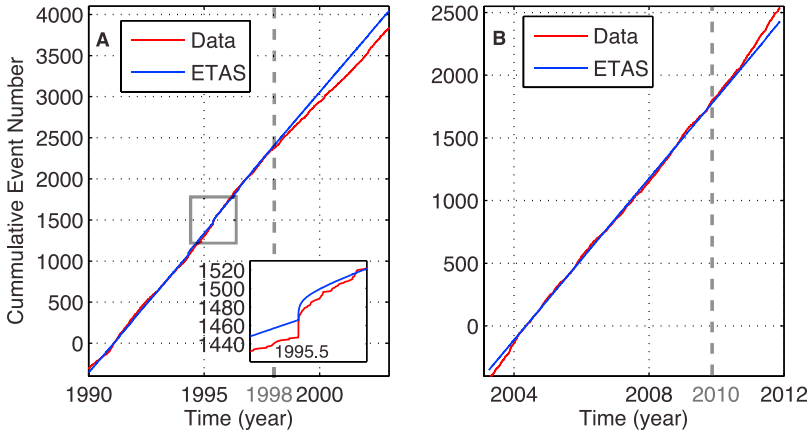

Figure 3. Results of optimization of the ETAS model for the pre-Denali and post-Denali 2002 earthquake catalog comparing the cumulative number of events. The observed data are shown in red and the ETAS prediction in blue. The ETAS model is optimized between 1990–1995.5 and extrapolated for the rest of the catalog except around the Denali earthquake. (a) For the pre-Denali data, the magnitude of completeness is 1.9. A significant deviation from the ETAS prediction occurs in 1998 and shows that the seismicity rate between 1990 and 1998 was significantly higher than between 1998 and 2002. The inset figure shows an earthquake near 1995.5 (b) For the post-Denali data, the magnitude of completeness is 1.5. Seismicity rate is approximately constant until mid 2010 when the rate increases. A deviation from the ETAS prediction occurs near the beginning of the slow slip event (mid 2010).

to the catalog during the training time period including the size and duration of the few modest aftershock sequences in the catalog (Figure 3a). Thus, we use them to model the catalog in the post-Denali earthquake time frame.

[18] The ETAS parameters were then used to model the expected seismicity rate in both the 1990–2002, and 2003–2011 time periods (Figure 3). While the parameters from the training period (1990–1995.5) fit the 2003–2010 time period well, there is an increase in background seismicity rate beginning in mid-2010 (Figure 3b) that is not consistent with these ETAS parameters and coincides in space and time with the slow slip event. The ETAS results also indicate that the background seismicity rate between 1990 and 1998 was higher than between 1998 and 2002 (Figure 3a). While it is not a direct detection, this portion of the Alaska subduction zone appears similar to the Boso section of the Japan Trench, which is well fit by ETAS in general, except for small amounts of 'extra' micro-seismicity that occurs repeatedly during slow-slip events and is manifested in a change in the background-rate parameter of the ETAS model [*Llenos et al.*, 2009]. The variations in the ETAS background rate parameter on ~5 year time scales (1990–1998, 1998–2002, 2004–2009, 2010–2011) provides indirect evidence that long duration, low-amplitude SSEs similar to the current 2010–2011 event, may occur regularly on this portion of the plate interface.

7. Discussion

[19] A change in velocity in 2004 at the same stations but in the opposite direction for which we found the slip transient in this study has recently been documented [*Freymueller*, 2012]. His interpretation for the 2004 velocity change is a locking event, in which a large patch on the subduction plate interface that had been creeping stopped for a few years, and then began creeping again [*Freymueller*, 2012]. Our results agree with his in the sense that the additional creep released energy equivalent to a SSE with a seismic moment of *Mw* 6.9 in 23 months. The combination of the geodetic and seismicity data implies that the time history of slow slip on the plate interface varies with a timescale of a few years.

[20] Non-volcanic tremor (NVT) related to the 1998–2001 SSE reported by *Ohta et al.* [2006] has been observed in south central Alaska. *Peterson and Christensen* [2009] documented the occurrence of NVT in south central Alaska for 3 months of each year between 1999 and 2001. The majority of the NVT signals lasted between 10 and 15 min. By the summer of 2001 episodes rarely lasted up to 10 min and the number of NVT episodes decreased significantly from the previous summers. This decreasing of NVT activity is coincident with the ending of a 3-year long SSE between 1998 and 2001 [*Ohta et al.*, 2006] and occurred at the same location. The temporal and spatial correlation between the NVT and SSE suggests the relationship between the two phenomena seen in Cascadia and southwest Japan also exists in Alaska. Currently, there is no report of increasing NVT related to the 2010 SSE we have observed.

[21] The duration of the SSE observed in this work is relatively long (>23 months). The Tokai region in central Japan and the southern Hikurangi margin in New Zealand are the only known subduction zones that produce SSEs of such long duration. *Ozawa et al.* [2002] reported an 18-month long slow slip event with an accumulated magnitude of 6.7 in the Tokai region. *Wallace and Beavan* [2010] reported three events since 2004 with a duration ranging from 200 to 492 days and magnitude 6.3 to 7.2. An interesting target for future study will be to understand the connection between the occurrence of such long duration slow-slip events and low-aftershock productivity in the 30–50 km depth range. Low aftershock productivity is indicative of low $A\sigma$ [*Dieterich*, 1994], where A is a friction parameter and σ is effective normal stress in the rate-state seismicity model and hence

may be a confirmation of the hypothesis that slow-slip events occur in regions of very low effective normal stress [*Liu and Rice*, 2007].

8. Conclusions

[22] We found a slow slip event in the south central Alaska subduction zone by applying the Network Strain Filter to PBO GPS data. The slow slip event started in early 2010 and is still in progress as of 30 November 2011. The modeled maximum subduction interface slip of 17 mm occurred beneath the Cook Inlet. The accumulated magnitude is about *Mw* 6.9 as of 30 November 2011. We also observed a slight seismicity increase that correlates to the SSE in space and time. In addition, a similar variation in seismicity rate has occurred in the past and suggests the possibility of earlier slow slip events in the same region, including but not limited to the one reported by *Ohta et al.* [2006].

[23] **Acknowledgments.** We thank Jeff Freymueller for valuable discussions. Reviews from Gina Schmalzle and an anonymous reviewer are highly appreciated. This research was supported by NSF EarthScope awards 0952174 (MW and JJM) and 0952249 (ER).

[24] The Editor thanks Gina Schmalzle and an anonymous reviewer for assisting in the evaluation of this paper.

References

Anderson, G. (2004), *Plate Boundary Observatory Data Management Plan*, UNAVCO, Boulder, Colo.

Beroza, G. C., and S. Ide (2011), Slow earthquakes and nonvolcanic tremor, *Annu. Rev. Earth Planet. Sci.*, *39*(1), 271–296, doi:10.1146/annurev-earth-040809-152531.

Christensen, D. H., and S. L. Beck (1994), The rupture process and tectonic implications of the great 1964 Prince William Sound earthquake, *Pure Appl. Geophys.*, *142*, 29–53, doi:10.1007/BF00875967.

Coleman, T. F., and Y. Y. Li (1996), A reflective Newton method for minimizing a quadratic function subject to bounds on some of the variables, *SIAM J. Optim.*, *6*, 1040–1058, doi:10.1137/S1052623494240456.

Dieterich, J. (1994), A constitutive law for rate of earthquake production and its application to earthquake clustering, *J. Geophys. Res.*, *99*(B2), 2601–2618, doi:10.1029/93JB02581.

Du, W., L. R. Sykes, B. E. Shaw, and C. H. Scholz (2003), Triggered aseismic fault slip from nearby earthquakes, static or dynamic effect?, *J. Geophys. Res.*, *108*(B2), 2131, doi:10.1029/2002JB002008.

Fialko, Y., D. Sandwell, M. Simons, and P. Rosen (2005), Three-dimensional deformation caused by the Bam, Iran, earthquake and the origin of shallow slip deficit, *Nature*, *435*, 295–299, doi:10.1038/nature03425.

Freymueller, J. T. (2012), Observation of a "Locking Event": A newly observed transient variation in the pattern of slip deficit at the Alaska Subduction Zone, *Seismol. Res. Lett.*, *83*, 433.

Fukuda, J., T. Higuchi, S. Miyazaki, and T. Kato (2004), A new approach to time-dependent inversion of geodetic data using a Monte Carlo mixture Kalman filter, *Geophys. J. Int.*, *159*, 17–39, doi:10.1111/j.1365-246X.2004.02383.x.

Fukuda, J., S. Miyazaki, T. Higuchi, and T. Kato (2008), Geodetic inversion for space-time distribution of fault slip with time-varying smoothing regularization, *Geophys. J. Int.*, *173*, 25–48, doi:10.1111/j.1365-246X.2007.03722.x.

Furumoto, A. S. (1965), Analysis of Rayleigh wave, part II, in *Source Mechanism Study of the Alaska Earthquake and Tsunami of March 27, 1964*, *Rep. HIG-65-17*, pp. 31–42, Inst. of Geophys., Univ. of Hawaii at Manoa, Honolulu.

Hayes, G. P., D. J. Wald, and R. L. Johnson (2012), Slab1.0: A three-dimensional model of global subduction zone geometries, *J. Geophys. Res.*, *117*, B01302, doi:10.1029/2011JB008524.

Itaba, S., and R. Ando (2011), A slow slip event triggered by teleseismic surface waves, *Geophys. Res. Lett.*, *38*, L21306, doi:10.1029/2011GL049593.

Johnson, M., K. Satake, S. R. Holdahl, and J. Sauber (1996), The 1964 Prince William Sound earthquake: Joint inversion of tsunami and geodetic data, *J. Geophys. Res.*, *101*, 523–532, doi:10.1029/95JB02806.

Kanamori, H. (1977), The energy release in great earthquakes, *J. Geophys. Res.*, *82*, 2981–2987, doi:10.1029/JB082i020p02981.

Liu, Y., and J. R. Rice (2007), Spontaneous and triggered aseismic deformation transients in a subduction fault model, *J. Geophys. Res.*, *112*, B09404, doi:10.1029/2007JB004930.

Llenos, A. L., J. J. McGuire, and Y. Ogata (2009), Modeling seismic swarms triggered by aseismic transients, *Earth Planet. Sci. Lett.*, *281*(1–2), 59–69, doi:10.1016/j.epsl.2009.02.011.

McGuire, J. J., and P. Segall (2003), Imaging of aseismic fault slip transients recorded by dense geodetic networks, *Geophys. J. Int.*, *155*, 778–788, doi:10.1111/j.1365-246X.2003.02022.x.

Miyazaki, S., J. J. McGuire, and P. Segall (2003), A transient subduction zone slip episode in southwest Japan observed by the nationwide GPS array, *J. Geophys. Res.*, *108*(B2), 2087, doi:10.1029/2001JB000456.

Murray, J. R., and P. Segall (2005), Spatiotemporal evolution of a transient slip event on the San Andreas fault near Parkfield, California, *J. Geophys. Res.*, *110*, B09407, doi:10.1029/2005JB003651.

Murray, J. R., P. Segall, P. Cervelli, W. Prescott, and J. Svarc (2001), Inversion of GPS data for spatially variable slip-rate on the San Andreas Fault near Parkfield, CA, *Geophys. Res. Lett.*, *28*(2), 359–362, doi:10.1029/2000GL011933.

Ogata, Y. (1988), Statistical models for earthquake occurrences and residual analysis for point processes, *J. Am. Stat. Assoc.*, *83*(401), 9–27.

Ohta, Y., J. Freymueller, S. Hreinsdottir, and H. Suito (2006), A large slow slip event and the depth of the seismogenic zone in the south central Alaska subduction zone, *Earth Planet. Sci. Lett.*, *247*(1–2), 108–116, doi:10.1016/j.epsl.2006.05.013.

Ohtani, R., J. J. McGuire, and P. Segall (2010), Network strain filter: A new tool for monitoring and detecting transient deformation signals in GPS arrays, *J. Geophys. Res.*, *115*, B12418, doi:10.1029/2010JB007442.

Okada, Y. (1985), Surface deformation due to shear and tensile faults in a half-space, *Bull. Seismol. Soc. Am.*, *75*(4), 1135–1154, doi:10.1016/0148-9062(86)90674-1.

Ozawa, S., M. Murakami, M. Kaidzu, T. Tada, T. Sagiya, Y. Hatanaka, H. Yarai, and T. Nishimura (2002), Detection and monitoring of ongoing aseismic slip in the Tokai region, central Japan, *Science*, *298*(5595), 1009–1012, doi:10.1126/science.1076780.

Ozawa, S., S. Miyazaki, Y. Hatanaka, T. Imakiire, M. Kaidzu, and M. Murakami (2003), Characteristic silent earthquakes in the eastern part of the Boso peninsula, Central Japan, *Geophys. Res. Lett.*, *30*(6), 1283, doi:10.1029/2002GL016665.

Peterson, C. L., and D. H. Christensen (2009), Possible relationship between nonvolcanic tremor and the 1998–2001 slow slip event, south central Alaska, *J. Geophys. Res.*, *114*, B06302, doi:10.1029/2008JB006096.

Schwartz, S. Y., and J. M. Rokosky (2007), Slow slip events and seismic tremor at circum-Pacific subduction zones, *Rev. Geophys.*, *45*, RG3004, doi:10.1029/2006RG000208.

Segall, P., and M. Matthews (1997), Time dependent inversion of geodetic data, *J. Geophys. Res.*, *102*, 22,391–22,409, doi:10.1029/97JB01795.

Wallace, L. M., and J. Beavan (2010), Diverse slow slip behavior at the Hikurangi subduction margin, New Zealand, *J. Geophys. Res.*, *115*, B12402, doi:10.1029/2010JB007717.

Wyatt, F. K. (1989), Displacement of surface monuments: Vertical motion, *J. Geophys. Res.*, *94*(B2), 1655–1664, doi:10.1029/JB094iB02p01655.

Zweck, C., J. T. Freymueller, and S. C. Cohen (2002), Three-dimensional elastic dislocation modeling of the postseismic response to the 1964 Alaska earthquake, *J. Geophys. Res.*, *107*(B4), 2064, doi:10.1029/2001JB000409.